Clim. Past Discuss., 10, 1265–1303, 2014
www.clim-past-discuss.net/10/1265/2014/
doi:10.5194/cpd-10-1265-2014

Climate of the Past
Discussions
Open Access

Variations in intermediate and deep ocean circulation in the subtropical northwestern Pacific from 26 ka to present based on a new calibration for Mg/Ca in benthic foraminifera

Y. Kubota[1], K. Kimoto[2], T. Itaki[3], Y. Yokoyama[4], Y. Miyairi[4], and H. Matsuzaki[5]

[1]Department of Geology and Paleontology, National Museum of Nature and Science, 4-1-1, Amakubo, Tsukuba, Ibaraki 305-0005, Japan
[2]Research Institute for Global Change, Japan Agency for Marine-Earth Science and Technology, 2-15 Natsushima-cho, Yokosuka, Kanagawa 237-0061, Japan
[3]Geological Survey of Japan, National Institute of Advanced Industrial Science and Technology, Central 7, Higashi 1-1-1, Tsukuba, Ibaraki 305-8567, Japan
[4]Atmosphere and Ocean Research Institute, The University of Tokyo, Tokyo, Japan
[5]Department of Nuclear Engineering and Management, The University of Tokyo, Tokyo, Japan

Received: 27 February 2014 – Accepted: 27 February 2014 – Published: 28 March 2014

Correspondence to: Y. Kubota (yoshimi@kahaku.go.jp)

Published by Copernicus Publications on behalf of the European Geosciences Union.

Abstract

To understand variations in intermediate and deep ocean circulation in the North Pacific, bottom water temperatures (BWT), carbon isotopes ($\delta^{13}C$) of benthic foraminifera, and oxygen isotopes ($\delta^{18}O$) of seawater at a water depth of 1166 m were reconstructed from 26 ka to present. A new regional Mg/Ca calibration for the benthic foraminifera *Cibicidoides wuellerstorfi* was established to convert the benthic Mg/Ca value to BWT, based on twenty-six surface sediment samples and a core top sample retrieved around Okinawa Island. In addition, core GH08-2004, retrieved from 1166 m water depth east of Okinawa Island, was used to reconstruct water properties from 26 ka to present. During the Last Glacial Maximum (LGM), from 24 to 18 ka, BWT appeared to be relatively constant at approximately 2 °C, which is ~ 1.5–2 °C lower than today. One of the prominent features of our BWT records was a millennial-scale variation in BWT during the last deglaciation, with BWT higher during Heinrich event 1 (H1; ~ 17 ka) and the Younger Dryas (YD; ~ 12 ka) and lower during the Bølling/Allerød (B/A; ~ 14 ka). The record of seawater $\delta^{18}O$ in core GH08-2004 exhibited a rapid increase in association with the rapid warming of BWT at 17 ka, likely due to the reduced precipitation in the North Pacific in response to less moisture transport from the equatorial Atlantic as a result of the collapse of the Atlantic Meridional Overturning Circulation. During the interval from 17 to 15 ka, the bottom water temperature tended to decrease in association with a decrease in the carbon isotope values of *C. wuellerstorfi,* likely as a result of increased upwelling of the older water mass that was stored in the abyssal Pacific during the glacial time. The timing of the increased upwelling coincided with the deglacial atmospheric CO_2 rise initiated at ~ 17 ka, and suggested that the increased upwelling in the subtropical northwestern Pacific from 17 to 15 ka contributed to the carbon release from the Pacific into the atmosphere.

Discussion Paper | Discussion Paper | Discussion Paper | Discussion Paper |

CPD
10, 1265–1303, 2014

Variations in intermediate and deep ocean circulation

Y. Kubota et al.

1 Introduction

Intermediate and deep water circulation in the Pacific is of particular interest because the deep Pacific is potentially an area where a large amount of carbon was stored during glacial times (Broecker et al., 2004, 2008). It is hypothesized that during the last glacial period, older carbon was released to the atmosphere from the deep Pacific through changes in ocean circulation. Thus, reconstruction of intermediate and deep ocean circulation in the North Pacific and its link to CO_2 release into the atmosphere is essential for understanding the mechanisms of glacial–interglacial climate change. At present, deep water formation is absent in the North Pacific because of excess precipitation and subsequent low surface salinity in the subarctic (e.g., Warren, 1983). Instead, the presence of intermediate water in the North Pacific (North Pacific Intermediate Water; NPIW) is seen as a well-defined salinity minimum in the subtropical North Pacific at depths of approximately 300–800 m (e.g., Sverdrup et al., 1942; Reid, 1965; Talley, 1993; Yasuda, 1997). In paleoceanographic field, several studies have been conducted on the subarctic, including the western North Pacific (Ahagon et al., 2003; Sagawa and Ikehara, 2008), Okhotsk Sea (Ohkushi et al., 2003), Bering Sea (Horikawa et al., 2010; Rella et al., 2012), and the eastern North Pacific (Kienast et al., 2006). Together, this body of work has improved our understanding of intermediate and deep water formation and deep ocean circulation in the North Pacific since the Last Glacial Maximum (LGM). During the LGM, a center of high-nutrient water, recognized by the lowest benthic carbon isotope data, existed ~ 3000 m water depth, which is ~ 1000 m deeper than the level of a similar layer today (Keigwin, 1998; Matsumoto et al., 2002). Based on depth differences in ^{14}C concentrations in the subarctic area, Okazaki et al. (2011) advocated that Pacific circulation shifted from a glacial stratified mode to an interglacial upwelling mode during the transition between Heinrich event 1 (H1) and the Bølling/Allerød (B/A). Paleoceanographic studies based on sedimentary records from the last deglaciation suggest that deep water was formed in the North Pacific and ventilated to a depth of ~ 2500–3000 m during H1 with the establishment

CPD
10, 1265–1303, 2014

of a deep Pacific Meridional Overturning Circulation (PMOC), a finding also supported by modeling results (Okazaki et al., 2011). The establishment of the PMOC was led by a collapse of the Atlantic Meridional Overturning Circulation (AMOC) that occurred after a large freshwater discharge into the high latitude North Atlantic. During H1, the NPIW was stronger and well-ventilated, and the area of formation was expanded to the Bering Sea, but the formation became weaker during the B/A (Rella et al., 2012). On the other hand, the contribution to the eastern equatorial Pacific of the Southern Ocean water masses, such as the Antarctic Intermediate Water (AAIW) and Antarctic Mode Water, increased during the LGM, Heinrich stadials 2 and 1, and the Younger Dryas (YD) (Pena et al., 2013). Recently, Chikamoto et al. (2012) presented simulation results conducted using two climate models: a coupled atmosphere–ocean general circulation model (MIROC) and an earth system model of intermediate complexity (LOVECLIM). Both models simulated subthermocline and intermediate water warming in the subtropical Pacific Ocean as a response to the collapse of the AMOC, although there was a difference between the two simulations in how much deep water formed. In spite of the importance of understanding intermediate and deep ocean conditions in the subtropical Pacific, proxy records of temperature and salinity at intermediate depths are rare in this region. Carbon isotopes of benthic foraminifera ($\delta^{13}C_C$) are regarded as a tracer of the water mass, thus, are useful for detecting changes in ocean circulation. Here, we present intermediate temperature and salinity records based on benthic foraminifera magnesium/calcium ratios (Mg/Ca) as well as oxygen and carbon isotope records that reveal the temporal variations of deep and intermediate waters in the North Pacific from 26 ka to present.

2 Oceanographic settings and water tracers

The North Pacific can be divided into the subtropical and subarctic gyres at ~35–40° N. On the surface, the western boundary current, Kuroshio, flows northward along the western side of the North Pacific and carries warm, saline, and oligotrophic

CPD
10, 1265–1303, 2014

water to the high latitudes, while the Oyashio flows southward and transports cold and more eutrophic water away from the high latitudes. There are three main water types at intermediate depths (500–1000 m) in the Pacific Ocean: the NPIW, AAIW and Equatorial Pacific Intermediate Water (EqPIW) (e.g., Bostock et al., 2010). The distribution and flow of the intermediate water masses are shown in Fig. 1. The NPIW is characterized by low salinity (33.9–34.1 PSU) and low oxygen concentrations (50–150 $\mu mol\,kg^{-1}$). At present, this water mass is formed in the Okhotsk Sea, subducts into and below the thermocline of the Kuroshio Extension, enters the subtropical gyres (Reid, 1965; Kaneko et al., 2001), and is distributed at intermediate depths in the North Pacific (Talley et al., 1993). In the west, a tongue of the NPIW extends into the Celebes Sea (Bingham and Lukes, 1995), while in the east, the NPIW is restricted to the subtropical gyre by the broad California Current (Talley, 1993). The AAIW is a distinctive water mass with high oxygen concentrations (200–250 $\mu mol\,kg^{-1}$) and relatively low salinity (34.3–34.5 PSU) (Bostock et al., 2010) as shown in Fig. 2. The formation of AAIW is linked to the Subantarctic Mode Waters and occurs in the southeast Pacific off southern Chile (Tally, 1996; Tsuchiya and Tally, 1998; Hanawa and Tally, 2001). The AAIW flows west into the Coral Sea, while another tongue enters the northern Tasman Sea (Wyrtki, 1962). EqPIW is distributed in the equatorial and tropical Pacific at intermediate depths (< 1000 m). Based on quasi-conservative tracers, such as radiocarbon ($\delta^{14}C$), EqPIW is a combination of parental AAIW waters mixed with old upwelling Pacific Deep Water (PDW) (Bostock et al., 2010). The lowest values of $\delta^{14}C$ in the EqPIW indicate that it is the oldest intermediate water in the Pacific (Bostock et al., 2010). However, the EqPIW displays latitudinal asymmetry, with higher silicate, higher phosphate, and lower oxygen concentrations in the northern part (Fig. 2). As a result, it is split into North (NEqPIW) and South (SEqPIW), which are separated at $\sim 2^{\circ}$ N (Bostock et al., 2010). The higher silicate in the NEqPIW likely originates from the NPIW (Sarmient et al., 2004), while the lower silicate in the SEqPIW is sourced from the Antarctic Surface Water via the AAIW and the equatorial undercurrent (Toggweiler et al., 1991).

Discussion Paper | Discussion Paper | Discussion Paper | Discussion Paper |

CPD

10, 1265–1303, 2014

Variations in intermediate and deep ocean circulation

Y. Kubota et al.

The study area was located east of Okinawa Island in the northern part of the Philippine Sea, which lies on the western side of the North Pacific and is composed of three basins: the Shikoku, Philippine, and West Mariana Basins (Fig. 3). The general circulation regime changes at around 1500 m depth in the Philippine Sea (Kaneko et al., 2001). Above this depth, the clockwise subtropical gyre is dominant with multiple zonal inflows of intermediate waters from western and southwestern areas. The NPIW flowing into the Philippine Sea crosses the Izu–Ogasawara–Mariana–Yap Ridge with total flows of $11 \times 10^9\,\mathrm{kg\,s^{-1}}$. Of this, $8 \times 10^9\,\mathrm{kg\,s^{-1}}$ circulates within the subtropical gyre along the Kuroshio, while the remainder is transported to the tropics and the South China Sea (Kaneko et al., 2001). There is input from the AAIW through the western boundary currents, recognized by high oxygen concentrations (Komatsu et al., 2004; Yasuda, 2004). Intermediate water in the Philippine Sea enters the South China Sea through the Luzon Strait (Qu et al., 2006), and is recognized as the NPIW by lower salinities between 400 and 1000 m water depth (Huang et al., 2013). Below 1500 m, the PDW from the eastern tropical Pacific and deep water from the South Pacific enter the Philippine Sea, and flow out north of 15° N, forming a large clockwise gyre (Kaneko et al., 2001). The salinity profile at the site GH08-2004 is shown in Fig. 4 (Itaki et al., 2009b) and exhibits the salinity minima (34.2–34.3 PSU), which is indicative of the influence of the NPIW, at 600–700 m water depth. However, the salinity becomes increasing at a depth of 800 m, indicating the decreasing contribution of the NPIW and the increasing contribution of the NEqPIW. The present salinity at the bottom of the site GH08-2004 is 34.5 PSU, which is within the salinity value of NEqPIW (34.5–34.6 PSU; Bostock et al., 2010). Thus, the bottom of the site is occupied mainly by NEqPIW with small contributions of NPIW and possibly AAIW.

Carbon isotope values ($\delta^{13}C$) of dissolved inorganic carbon (DIC) have been utilized as water mass tracers. The $\delta^{13}C$ values of DIC ($\delta^{13}C_{DIC}$) at intermediate or deep water depths are mainly controlled by mixing and ages of the water masses, as well as surface water processes such as biological productivity and air–sea exchange (e.g., Lisiecki, 2010). Because lighter ^{12}C is preferentially taken up by phytoplankton to form

CPD
10, 1265–1303, 2014

Variations in intermediate and deep ocean circulation

Y. Kubota et al.

organic carbon at the surface, $\delta^{13}C_{DIC}$ generally shows higher values at the ocean surface. Thus, $\delta^{13}C$ distribution has an inverse relationship to nutrient concentrations. As ^{13}C-depleted organic carbon sinks and remineralizes at depth, it decreases $\delta^{13}C_{DIC}$ of deep water. Modern $\delta^{13}C_{DIC}$ data show a clear separation depending on the water masses, with NPIW (−0.5–0 ‰) < NEqPIW (−0.25–0.25 ‰) < SEqPIW (0–0.5 ‰) < AAIW (0.75–1.75 ‰) (Bostock et al., 2010). The distribution of the $\delta^{13}C_{DIC}$ is comparable to the phosphate distribution in the Pacific (Fig. 2b). The $\delta^{13}C$ of epifaunal benthic foraminifera living at the bottom water–surface sediment interface is used to estimate changes in water mass $\delta^{13}C_{DIC}$ composition, and *Cibicidoides* reflect $\delta^{13}C_{DIC}$ in ambient water with a defined genera- or species-dependent offset in $\delta^{13}C_C$ (Graham et al., 1981; McCorkle et al., 1990, 1997).

3 Samples and location

3.1 Surface sediments and core GH08-2004

Twenty-six surface sediments were recovered from the area around Okinawa Island using a Kinoshita-Grab sampler (K-Grab) during the GH08, GH09, and GH10 cruises of the Geological Survey of Japan on R/V *Hakurei-maru No. 2* (Fig. 3; Itaki et al., 2009a, 2010, 2011a). The samples were from a wide range of water depths, from ∼ 300 to 2700 m. These sediments consisted of sandy mud to mud (Table 1), and locations of the surface samples were carefully selected and restricted to the area where reworking or sediment transport from shallower areas (such as turbidites) were unlikely to have occurred (Fig. 3). In situ bottom water temperatures and salinities were measured using an Idronaut Ocean Seven 306 CTD system attached to the K-Grab sampler. These surface sediments and one additional core top sample were used to calibrate benthic Mg/Ca with bottom water temperature (Table 1).

CPD
10, 1265–1303, 2014

A gravity core (GH08-2004, with a length of 2.73 m) was recovered from the continental slope east of Okinawa Island (26°12.86′ N, 128°14.17′ E, 1166 m water depth). An olive-colored oxidation layer was identified in the upper 8 cm of the core (Itaki et al., 2009a), while the lower part of the core consisted of olive to gray silty clay with some patches of sand. A brownish-gray tephra layer was recognized at 43 cm beneath the seafloor, and was identified as the K–Ah tephra (7.3 ka; Kitagawa et al., 1995) based on chemical analyses using an electron probe micro-analyzer (Itaki et al., 2009a). The core material was sampled at 2.2 cm intervals, and approximately 10–20 cm^3 sediment samples were used for the chemical analyses of the foraminifera tests in this study.

3.2 Benthic foraminifera *Cibicidoides wuellerstorfi*

The benthic foraminifera genus *Cibicidoides* is widely used in paleoceanographic reconstructions because of its epifaunal habitat and wide distribution. Mg/Ca calibration equations have been proposed for several *Cibicidoides* species, such as *C. pachyderma, C. wuellerstorfi,* and *C. compressus* (Rosenthal et al., 1997; Lear et al., 2002; Martin et al., 2002). Although *C. wuellerstorfi* was recognized in most of the surface sediments used in this study, the other *Cibicidoides* species were rare. *C. wuellerstorfi* observed in this study had two types of surface textures: one was sensu stricto and had a relatively smooth surface texture (type A), while the other was characterized by a rough and overgrown surface (type B) (Fig. 5). It is highly unlikely that the overgrown surface of the type B results from the secondary calcite deposition based on the SEM images. *C. wuellerstorfi* type B was more abundant than *C. wuellerstorfi* type A in most of the surface and core samples, and the Mg/Ca temperature calibration equations were generated for *C. wuellerstorfi* type B because of their higher abundance and continuous occurrence in core sediments. *C. wuellerstorfi* type B was also used for the oxygen and carbon isotope time series. The oxygen and carbon isotopes of *C. wuellerstorfi* type A were also measured for 28 horizons, but Mg/Ca measurements were not performed due to inadequate sample sizes.

CPD
10, 1265–1303, 2014

4 Analytical methods

Approximately 10–20 cm^3 of the K-Grab and core materials were washed onto a 63 µm mesh sieve and dried in the oven at 50 °C for one day. To minimize the error introduced by individual specimen heterogeneity, as many foraminifera tests as possible were picked from each sediment sample. Four to twenty well-preserved and clean individual *C. wuellerstorfi* were picked from the > 250 µm size fraction for Mg/Ca and isotope analyses. Cleaning steps based on Boyle and Keigwin (1985) were carried out prior to analyses with some slight modifications. All cleaning steps were conducted in a class 10 000 laminar flow clean bench at the Research Institute for Global Change (RIGC), Japan Agency for Marine-Earth Science and Technology (JAMSTEC). First, foraminiferal tests were crushed on a glass slide and placed into a micro tube where they were repeatedly washed using ultra pure (Milli-Q) water (> 18.3 MΩ) and methanol in an ultrasonic bath. Then, the samples were divided into two micro tubes, for isotopes and Mg/Ca analyses. For the Mg/Ca samples, additional cleaning steps were conducted: clay materials, organic matter, and Mn–Fe oxides were removed using a reductive and oxidative procedure (Boyle, 1994). The $\delta^{18}O$ and $\delta^{13}C$ of benthic foraminifera *C. wuellerstorfi* ($\delta^{18}O_c$ and $\delta^{13}C_c$ respectively) was measured using a Finnigan-MAT-252 mass spectrometer (IR–MS) with a Kiel carbonate device at the Mutsu Institute for Oceanography (MOI), JAMSTEC. The $\delta^{18}O_c$ and $\delta^{13}C_c$ was determined by analysis of carbon dioxide generated from foraminifera tests by reaction with 100 % phosphoric acid at 70 °C and introduced to the mass spectrometer. The reproducibility of the measurement was better than ±0.05 ‰ (1σ) for $\delta^{18}O$ and $\delta^{13}C$, as determined by replicate measurements of international standards NBS-19 (RM8544 Limestone). Mg/Ca analysis was performed using a Thermoquest ELEMENT-2 multi-sector inductively coupled plasma mass spectrometer (HR–ICP–MS) at the MOI, JAMSTEC. After the cleaning procedure, for two out of twenty-seven samples, the foraminiferal testes were repicked and prepared for duplication analyses. For twenty out of twenty-seven samples, another set of the samples was prepared in order to improve

CPD
10, 1265–1303, 2014

the reliability of the Mg/Ca values. Four isotopes of three trace elements (^{24}Mg, ^{44}Ca, ^{48}Ca, ^{55}Mn) were analyzed using Sc as the internal standard. Four working standards were prepared by successive dilutions of the stock standard solutions to match the concentrations of Ca (20 ppb to 5 ppm) and Mg (0.05–10 ppb) covering the ranges of the Ca and Mg concentrations found in all of the samples. Mn/Ca was monitored to check for possible diagenetic overgrowths (Boyle, 1983) but was below 65 µmol mol^{-1} for most of the samples, indicating a negligible influence of diagenesis on Mg/Ca. The precision of replicate analyses of the working standard for Mg/Ca in one sequence was better than ±0.03 mmol mol^{-1}.

5 Age model for GH08-2004

Radiocarbon analysis (Table 2) was carried out by accelerator mass spectrometry (AMS) ^{14}C dating on approximately 6–12 mg of the planktonic foraminifera *Globigerinoides sacculifer, Globigerinoides ruber, Globorotalia menardii*, and *Globorotalia truncatulinoides* in addition to the results by Itaki (2010) and Itaki et al. (2011b). The foraminiferal tests were extracted from sediment samples in 10 core horizons. The conventional ^{14}C dates were converted to calendar ages using the Calib 6.0 software (Stuiver and Reimer, 1993) with the Intcal/Marine09 calibration curve (Reimer et al., 2009). A ΔR value of 44 ± 16 yr was used as the regional reservoir correction, which was derived from six locations (#1002 to #1007) in the Ryukyu Islands (Yoneda et al., 2007). The ^{14}C datum just above the K–Ah tephra at 43 cm was in good agreement with the age of the tephra (7.3 ka; Kitagawa et al., 1995). The ages of the sediment between the tie points were interpolated assuming linear sedimentation rates of ∼ 10–15 cm kyr^{-1} from 26 to 7.3 ka and ∼ 8 cm kyr^{-1} from 7.3 ka to present.

CPD
10, 1265–1303, 2014

6 Results

6.1 Mg/Ca temperature calibration

Mg/Ca values for the surface sediment samples ranged from 0.83 to 3.10 mmol mol^{-1} and showed a strong decrease with water depth and increase with bottom water temperature (BWT) (Table 1; Fig. 7). Twenty-seven *C. wuellerstorfi* Mg/Ca analyses were fitted to BWT. Since CTD measurements were not conducted at the core site, CTD data from the vicinity of the core site was used for the BWT of the core top samples. Although an exponential relationship between Mg/Ca and temperature is thermodynamically reasonable, some studies have reported that a linear fit is a more useful approximation (Toyofuku et al., 2000; Marchitto et al., 2007b). Exponential and linear regressions of *C. wuellerstorfi* Mg/Ca and temperature ranging from 1.7 to 16.3 °C yielded the following relationships:

$$\mathrm{Mg/Ca} = 0.84(\pm 0.02) \cdot \exp(0.083(\pm 0.003) \cdot \mathrm{BWT}) \quad (R^2 = 0.97, P < 0.001) \tag{1}$$

$$\mathrm{Mg/Ca} = 0.66(\pm 0.04) + 0.14(\pm 0.005) \cdot \mathrm{BWT} \quad (R^2 = 0.97, P < 0.001) \tag{2}$$

where the standard errors of the coefficients and intercepts are given in parentheses. The standard error derived from the new Mg/Ca data set was ±1.1 °C for the exponential regression and ±0.92 °C for the linear regression. Based on these equations, the precision of replicate Mg/Ca analyses of ±0.03 mmol mol^{-1} corresponded to ±0.2–0.3 °C, which was smaller than the standard error derived from the calibration data set. The slope of our equation was 8.3 % per °C for the exponential fitting, which was lower than previous studies that have indicated 11–28 % per °C (e.g., Healey et al., 2008). On the other hand, the linear fit to the same data set exhibited an Mg/Ca temperature dependence of 0.14 mmol mol^{-1} per °C. This slope was similar to the equations of Marchitto et al. (2007b) and Elderfield et al. (2006), which covered a wide temperature range but used different *Cibicidoides* species. Our y-intercept (0.66 mmol mol^{-1}) for the liner fit was 0.24 to 0.56 mmol mol^{-1} lower than

CPD
10, 1265–1303, 2014

those in previous studies. Overall, the observed Mg/Ca values were smaller than those expected for the same temperature using previously published regression lines. The difference in calibrated temperatures between our data set and previous studies was from 0.1–~2 °C (Martin et al., 2002; Lear et al., 2002; Elderfield et al., 2006). Thus, the application of the regional regression lines appears to be necessary. The smaller Mg/Ca values in this study may be due to species dependence and differences in shell surface textures among species. The effects of these factors on Mg/Ca incorporation has been reported, and *C. wuellerstorfi* exhibits the lowest Mg/Ca values among the *Cibicidoides* species (Elderfield et al., 2006). Martin et al. (2002) also pointed out that core top data for *Cibicidoides* species from sites with BWT below 3 °C in the Atlantic depart from the exponential equation derived from BWT between −1 and 18 °C and exhibit a steeper gradient in the Mg/Ca to temperature ratio. Elderfield et al. (2006) concluded that the lowered Mg/Ca at temperatures below ~3 °C coincides with a steep increase in the gradient of oceanic carbonate ion saturation ($\Delta[CO_3^{2-}]$) vs. temperature. If the data point from GH08-197 that shows a higher Mg/Ca value is omitted, a steeper gradient can be seen to exist in a narrow temperature range below 3 °C in this study (0.36 mmol mol^{-1} per °C; $R^2 = 0.71$) (Table 1). However, the magnitude of the $\Delta[CO_3^{2-}]$ effect could not be evaluated due to considerable uncertainty, including a narrow range in Mg/Ca, analytical error, and heterogeneity of the foraminifera tests, as discussed in Elderfield et al. (2006).

6.2 Downcore results

6.2.1 Benthic Mg/Ca-derived temperature variation

The Mg/Ca values for GH08-2004 varied between 0.61 and 1.45 mmol mol^{-1} from 26 ka to present (Fig. 8). Mg/Ca was relatively high at 25 ka, which likely coincided with Heinrich event 2 (H2). Mg/Ca showed the lowest value of ~0.8 mmol mol^{-1} during the LGM (24–17 ka). Unlike the benthic oxygen isotope ($\delta^{18}O_c$) record, obvious millennial-scale changes were superimposed on the glacial–interglacial-scale during the last

Discussion Paper | Discussion Paper | Discussion Paper | Discussion Paper |
CPD
10, 1265–1303, 2014
Variations in intermediate and deep ocean circulation

Y. Kubota et al.

deglaciation, with two peaks in Mg/Ca at 17–16.6 ka and 12–11 ka, likely coinciding with H1 and YD, respectively. A characteristic rapid increase followed by a slower decrease was observed in the Mg/Ca variations during H2 and H1. Mg/Ca began to decrease by $\sim 0.3\,\mathrm{mmol\,mol^{-1}}$ from 16.6 to 14 ka, and subsequently increased by $\sim 0.5\,\mathrm{mmol\,mol^{-1}}$ toward 11.5 ka. Holocene Mg/Ca was highly variable, ranging between ~ 0.8 and $\sim 1.2\,\mathrm{mmol\,mol^{-1}}$ on a multi-millennial scale, with a negative peak at 9.2 ka and a positive peak at ~ 8.2 ka. Negative peaks at 6.5 and 2.5 ka were also prominent.

Mg/Ca of foraminifera tests can be lowered by carbonate dissolution (Mekik et al., 2007), but the potential dissolution effects are unlikely to affect the changes in Mg/Ca values, as the core site was located well above the carbonate lysocline depth (~ 2000 m in the subtropical northwestern Pacific; Feely et al., 2004). The Mg/Ca values of core GH08-2004 were converted to temperature using Eq. (2) because Mg/Ca values lower than $1\,\mathrm{mmol\,mol^{-1}}$ cannot be converted to temperature using Eq. (1) (Fig. 9b). The lowest Mg/Ca value, which occurs at ~ 22 ka, gave a calibrated temperature of $-0.22\,^{\circ}$C. During the LGM, from 24 to 18 ka, BWT was relatively constant at approximately $2\,^{\circ}$C, which was ~ 1.5–$2\,^{\circ}$C lower than today (Fig. 4). This meant that the residual glacial–interglacial δ^{18}O differences could be mostly explained by the rise in BWT (0.24 ‰ per $^{\circ}$C; see Eq. 3). Subsequently, BWT increased to $\sim 3\,^{\circ}$C at 17 ka, then decreased to $\sim 1.8\,^{\circ}$C during the B/A, before starting to increase again at the onset of the YD. Even during the Holocene, the multi-millennial-scale variation was evident, decreasing from 4.8 to $1.7\,^{\circ}$C from the onset of YD to 9 ka, increasing to $4.4\,^{\circ}$C at 8.2 ka, and decreasing again to $2\,^{\circ}$C at 6.5 ka.

6.2.2 Benthic δ^{18}O and δ^{13}C variations

Because $\delta^{18}O_c$ and $\delta^{13}C_c$ of *C. wuellerstorfi* type A followed the $\delta^{18}O_c$ curve of *C. wuellerstorfi* type B (Fig. 8b and c), the difference between the two types of *C. wuellerstorfi* appeared to be negligible in terms of the isotopes. The benthic foraminifera $\delta^{18}O_c$ from core GH08-2004 showed a glacial transition, and gradually

CPD
10, 1265–1303, 2014

decreased from ~4.0 to ~2.5‰ from the LGM to the present (Fig. 8b). The 1.5‰ difference in $\delta^{18}O_c$ between the LGM and the present was 0.4–0.5‰ larger than that expected based on the global ice volume effect (Schrag et al., 2002), which indicated changes in temperature and/or local seawater $\delta^{18}O$ ($\delta^{18}O_w$) on the glacial–interglacial scale. The $\delta^{18}O$–temperature relationship for benthic foraminifera was reported by Shackleton (1974), and was derived from the original equation of isotopic fractionation between calcite and water established by O'Neil et al. (1969).

$$T = 16.9 - 4.38(\delta^{18}O_c - \delta^{18}O_w) + 0.10(\delta^{18}O_c - \delta^{18}O_w)^2 \quad (3)$$

The PDB scale is converted to the VSMOW scale as follows: ($\delta^{18}O_w$(VSMOW) = $\delta^{18}O_c$(PDB) + 0.27‰; Hut, 1987). Subsequently, the ice volume offset (Waelbroeck et al., 2002) is subtracted from $\delta^{18}O_w$, yielding the residual $\delta^{18}O_w$ ($\Delta\delta^{18}O_w$) (Fig. 9e). From 2 ka to present, $\delta^{18}O_w$ averaged −0.47‰, similar to the modern $\delta^{18}O_w$ value of −0.3 to −0.4‰ in the vicinity of the core site (Suzuki et al., 2010). The downcore $\Delta\delta^{18}O_w$ showed, on average, 0.4‰ lower values during the LGM than today, with large-amplitude millennial to multi-millennial fluctuations (± ~0.4‰) during the deglaciation and Holocene. Compared to the Mg/Ca results, higher $\Delta\delta^{18}O_w$ events at 17, 11.5, 10.2, and 8.2 ka basically coincided with warmer BWT peaks, while lower $\Delta\delta^{18}O_w$ events coincided with cooler BWT peaks (Fig. 9). The $\Delta\delta^{18}O_w$ shifted by −0.8‰ from 11.5 to 9.4 ka, increased by 0.9‰ toward 8.2 ka, and decreased again toward 6.6 ka. Although the temporal resolution was low during the middle and late Holocene, $\Delta\delta^{18}O_w$ showed an increasing trend in accordance with the increasing trend in Mg/Ca from 2 ka to present.

Average benthic $\delta^{13}C_c$ from 2 ka to present was 0.24‰, within the modern range of $\delta^{13}C_{DIC}$ from NEqPIW (−0.25–0.25‰). Downcore benthic $\delta^{13}C_c$ exhibited lower values during the LGM with negative peaks at 22.5 and 19.5 ka (Fig. 9). A negative shift in $\delta^{13}C_c$ from 17 to 14.5 ka was in accordance with the gradual decrease in BWT. The $\delta^{13}C_c$ then shifted to higher values at 13 ka, coinciding with the beginning of the

CPD
10, 1265–1303, 2014

YD. During the Holocene, $\delta^{13}C_c$ shifted by approximately 0.2 ‰ during the time from 8 to 7 ka, and showed a decreasing trend from 3 ka to present.

7 Discussion

7.1 Interpretation of proxy changes during the last deglaciation

One of the prominent features of our records was millennial-scale variation in BWT during the last deglaciation. The deglacial pattern of BWT at site GH08-2004 with warming and cooling in association with H1 and B/A, respectively, was opposite to that of the sea surface temperature (SST) in the mid-latitude northwestern Pacific (Sagawa and Ikehara, 2008) as well as the marginal seas such as the East China Sea (Sun et al., 2005; Kubota et al., 2010) and the South China Sea (Kiefer and Kienast, 2005) that show a warming synchronous with the B/A warming in Greenland ice cores (Fig. 9). In contrast, an SST record based on planktonic foraminifera Mg/Ca from the same core as our benthic record showed an approximately 1 °C increase at 17.5–17 ka (Lee et al., 2013), which coincided with the rapid warming of the intermediate water. However, the continued rise of SST in core GH08-2004 toward the B/A (Lee et al., 2013) is opposite to our BWT record that indicated a decreasing trend.

Recent modeling results based on both an earth model of intermediate complexity, LOVECLIM, and a CGCM MIROC simulated subthermocline and intermediate warming in the Pacific basin between 30° N and 30° S as a result of the collapse of the AMOC and consequent establishment of the PMOC (Chikamoto et al., 2012). The mechanism involved in the warming of intermediate depths in the tropical and subtropical Pacific is as follows: due to the PMOC intensification, a decrease in the PDW return flow and reduced upwelling from the abyssal Pacific would contribute to the warming of tropical intermediate waters (Chikamoto et al., 2012). The BWT warming estimate of ∼ 1 °C at the beginning of H1 found in core GH08-2004 was consistent with the simulation results. In addition, a small increase in $\delta^{13}C_C$ from 19 to 17 ka in core GH08-2004

CPD
10, 1265–1303, 2014

also suggested decreased upwelling of the deep water. However, another BWT record based on Mg/Ca of *Uvigerina akitaensis* from core GH02-1030 off northern Japan (42°13.77′ N, 144°12.53′ E, 1212 m water depth) exhibited a pattern opposite to our records, with warming at the beginning of the B/A, and subsequent cooling in the YD (Sagawa and Ikehara, 2008; Fig. 9c). This discrepancy was unlikely due to the uncertainty of the age models, because the age differences in the temperature peaks between the two cores were much larger than errors expected by ^{14}C measurements. Because the LOVECLIM H1 simulation showed an asymmetric intermediate water response with cooling in the subarctic and warming in the subtropical North Pacific (Chikamoto et al., 2012), it was likely that the subarctic and subtropical waters showed different temperature responses.

In contrast, the rapid decrease in $\Delta\delta^{18}O_w$ in association with the rapid BWT warming at 17 ka in core GH08-2004 was likely due to the reduced precipitation in the North Pacific in response to less moisture transport from the equatorial Atlantic as a result of the AMOC collapse (Okazaki et al., 2010; Chikamoto et al., 2012). The intensified PMOC would be maintained as a positive feedback, in accordance with the Stommel feedback scenario (Stommel, 1961) as intensified PMOC supplied the subtropical saline water to the high latitudes (Okazaki et al., 2010; Chikamoto et al., 2012). At that time, more heat was transported to the high latitudes in the North Pacific while less heat was transported in the North Atlantic (Okazaki et al., 2010). The large-scale surface cooling in the subarctic North Pacific would then intensify the Aleutian low in winter (Okumura et al., 2009) and lead to anomalous westerly winds in the mid-latitude North Pacific (Chikamoto et al., 2012). The intensified subtropical gyre, in accordance with the intensified subarctic gyre, could enhance the Kuroshio Current leading to greater heat transport to the high latitudes. Approximately 1 °C warming in SST at 17.5–17 ka in core GH08-2004 (Lee et al., 2013) could be explained by the intensified transport of warm water from the equatorial western Pacific.

After the rapid warming of the intermediate water, the gradual cooling in BWT from ~ 17 to 15 ka in core GH08-2004 occurred in association with a negative shift

CPD
10, 1265–1303, 2014

in the benthic $\delta^{13}C_c$, which suggested an increase in the upwelling of deep water. The gradual shift in $\Delta\delta^{18}O_W$ toward more negative values indicated freshening of the intermediate water that was likely due to an increasing ratio of precipitation to evaporation in the North Pacific.

The BWT began to increase again at 12.5 ka and reached the warmest temperature at 11.5 ka during the YD, approximately 1 kyr earlier than the surface water warming that ended at 10.6 ka. At the beginning of the YD, the benthic $\delta^{13}C_c$ increased as well. Although the pattern of the benthic $\delta^{13}C_c$ did not match perfectly to that of the BWT during the YD, both records suggested a temporal reduction of the deep water upwelling at the beginning of the YD.

7.2 Ocean circulation during the deglaciation

During the glacial time, the water mass corresponding to the modern NPIW was thought to be thicker and deeply penetrated into the North Pacific, the so-called Glacial North Pacific Intermediate Water (GNPIW) (Matsumoto et al., 2002; Okazaki et al., 2012). During a severe cold interval during the deglaciation, such as H1, its main source area was probably in the Bering Sea (Ohkushi et al., 2003; Horikawa et al., 2010; Rella et al., 2012), and spread south to the California margin in the eastern North Pacific (e.g., Keigwin and Jones, 1990; Behl and Kennett, 1996; Tada et al., 2000; Hendy and Pedersen, 2005; Okazaki et al., 2010). Okazaki et al. (2010) suggested that the GNPIW extended to ~ 2500 m and flowed southward along the western margin of the North Pacific during early H1. On the other hand, the increased meridional export of AAIW at ~ 18–17 ka is suggested based on a Nd isotope record of thermocline-dwelling planktonic foraminifera from the eastern equatorial Pacific (Fig. 9f; Pena et al., 2013). Evidence from the South China Sea also suggests that the increased influence of the AAIW peaked at ~ 16 ka during H1 based on the Nd isotopes of bulk sediment (Huang et al., 2012). Considering the relative contributions of the water masses to site GH08-2004, both the increased contribution of the GNPIW and the

AAIW could have compensated for the reduced upwelling of deep water during early H1. This relationship was repeated again at the beginning of the YD and reversed during the B/A. The influence of the intermediate water originating from the Southern Ocean began to decrease and the contribution of the PDW had been increasing in the eastern equatorial Pacific from 17.5 to 13 ka (Pena et al., 2013). This corresponded to a decreasing trend in BWT and $\delta^{13}C_c$ in core GH08-2004. The increase in upwelling that was interpreted from the intermediate cooling and low $\delta^{13}C_c$ was likely due to the reorganization of Pacific circulation that was related to reduction of the AAIW export to the tropics and less ventilation of GNPIW. Our interpretation is consistent with Okazaki et al. (2010), who claimed that, in the North Pacific, there was a shift from a stratified glacial mode during H1 to an upwelling interglacial mode during the B/A. However, it should be noted that our results also showed a temporal reversal to the relatively stratified mode at the beginning of the YD.

7.3 Implications for carbon storage in the Pacific during the deglaciation

Atmospheric CO_2 concentrations rose approximately 40 ppm during H1. This CO_2 is thought to have been stored in the abyssal Pacific and released into the atmosphere due to changes in ocean circulation (Broecker and Barker, 2007). So far, there has been still debate on the mechanism by which the old carbon was released into the atmosphere. Recent studies have found evidence for the existence of a large, old, CO_2-rich water mass in the abyssal Southern Ocean during the last glacial period (Skinner et al., 2010; Burke and Robinson, 2011). In contrast, work by Okazaki et al. (2012) compiled $\delta^{14}C$ records from several parts of the northwestern Pacific and concluded that there was no sign of massive mixing of old carbon from the abyssal reservoir during the glacial to deglacial period. Evidence for the upwelling of ^{14}C-depleted water was not found off the margin of Chile (De Pol-Holz et al., 2010) or the Drake passage either (Pahnke et al., 2008). On the other hand, eastern North Pacific records indicate injection of ^{14}C-depleted intermediate waters at ~ 16–15 ka off the west coast of Baja California (Marchitto et al., 2007a). In the eastern equatorial Pacific, the $\delta^{13}C$ minima

CPD
10, 1265–1303, 2014

of the thermocline-dwelling foraminifera at ~ 16–15 ka also have been documented at TR163-19 and ODP site 1240 (Spero and Lea, 2002; Pena et al., 2013). Considering the enhanced PDW signal (decreasing εNd) from 17.5 to 13 ka in the Nd isotope record in ODP site 1240 in the eastern equatorial Pacific (Pena et al., 2013), the simultaneous decreasing trend in $\delta^{13}C$ of the thermocline species in the eastern equatorial Pacific could be interpreted as increased upwelling of DIC-rich deep water. In the western side of the equatorial Pacific, boron isotope data suggests that the interval from ~ 18 to 13.8 ka is marked by surface water pCO_2 values that substantially exceed atmospheric pCO_2 (Palmer and Pearson, 2003). The surface water pCO_2 began to increase at ~ 18–17 ka and was highest at ~ 15 ka, which is in good agreement with the negative peak in our $\delta^{13}C$ records in the western subtropical and that in eastern equatorial Pacific (Spero and Lea, 2002; Pena et al., 2013). The upwelling in the tropical and subtropical Pacific and subsequent release of older carbon to the atmosphere likely contributed to the rise of atmospheric CO_2 during the time interval between 17 and 15 ka.

8 Conclusions

We measured benthic Mg/Ca, $\delta^{13}C$, and $\delta^{18}O$ in core GH08-2004, obtained at 1166 m in the subtropical northwestern Pacific. Based on the new benthic Mg/Ca temperature calibration, the BWT, benthic $\delta^{13}C$, and bottom water $\Delta\delta^{18}O_w$ were reconstructed from 26 ka to present. Our data indicated that the increase in BWT at the beginning of the cold intervals (H1 and YD) during the last deglaciation could be explained as a response to the AMOC collapse. The decreasing trend in BWT from 17 to 15 ka was associated with a decrease in benthic $\delta^{13}C$, interpreted as increased upwelling of the DIC-rich water from the deep Pacific that likely contributed to the atmospheric CO_2 rise during the early deglaciation. Our results emphasized the importance of the tropical and equatorial Pacific as the main area where upwelling and degassing of CO_2 occurred during this time.

CPD
10, 1265–1303, 2014

Acknowledgements. We sincerely thank the onboard scientists and crew of cruises GH08, GH09, and GH10 of R/V *Hakurei-maru No. 2* for their sampling assistance. We also thank Shiro Hasegawa and Hitomi Uchimura for identification of the benthic foraminifera. Analyses were supported by the staff at the Mustu Institute of Oceanography (MIO), including Hideki Yamamoto, Takamitsu Omura, and Noriyuki Kisen. This study was funded by Japan Society for the Promotion of Science (JSPS) Kakenhi, Grant Numbers 21740373, 25400504, and 23221022. This research was also supported by a grant from the Japan Agency for Marine-Earth Science and Technology (JAMSTEC) from the Ministry of Education, Culture, Sports, Science, and Technology (MEXT, Japan).

References

Ahagon, N., Ohkushi, K., Uchida, M., and Mishima, T.: Mid-depth circulation in the northwest Pacific during the last deglaciation: evidence from foraminiferal radiocarbon ages, Geophys. Res. Lett., 30, 2097, doi:10.1029/2003GL018287, 2003.

Barker, S., M. Greaves, and Elderfield, H.: A study of cleaning procedures used for foraminiferal Mg/Ca paleothermometry, Geochem. Geophy. Geosy., 4, 8407, doi:10.1029/2003GC000559, 2003.

Behl, R. J. and Kennett, J. P.: Brief interstadial events in the Santa Barbara Basin, NE Pacific, during the past 60 kyr, Nature, 379, 243–246, doi:10.1038/379243a0, 1996.

Bingham, F. M. and Lukas, R.: The distribution of intermediate water in the western equatorial Pacific during January–February 1986, Deep-Sea Res., 42, 1545–1573, 1995.

Bostock, H. C., Opdyke, B. N., and Williams, M. J. M.: Characterizing the intermediate depth waters of the Pacific Ocean using δ^{13}C and other geochemical tracers, Deep-Sea Res. Pt. I, 57, 847–859, 2010.

Boyle, E. A.: Manganese carbonate overgrowths on foraminiferal tests, Geochim. Cosmochim. Ac., 47, 1815–1819, 1983.

Boyle, E. A.: Acomparison of carbon isotopes and cadmium in the modern and glacial maximum ocean: can we account for the discrepancies?, in: Carbon Cycling in the Global Ocean: Constrains on the Ocean's Role in Global Change, edited by: Zahn, R., Pedersen, T. F., Kaminski, M.A, and Labeyrie, L., Springer-Verlag, New York, 167–194, 1994.

CPD
10, 1265–1303, 2014

Boyle, E. A. and Keigwin, L. D.: Comparison of Atlantic and Pacific paleochemical records for the last 215,000 years: changes in deep ocean circulation and chemical inventories, Earth Planet. Sc. Lett., 76, 135–150, 1985.

Broecker, W. and Barker, S.: A 190 ‰ drop in atmosphere's $\delta^{14}C$ during the "Mystery Interval" (17.5 to 14.5 kyr), Earth Planet. Sci. Lett., 256, 90–99, 2007.

Broecker, W., Barker, S., Clark, E., Hajdas, I., Bonani, G., and Stott, L.: Ventilation of the glacial deep Pacific Ocean, Science, 306, 1169–1172, 2004b.

Broecker, W., Clark, E., and Barker, S.: Near constancy of the Pacific Ocean surface to mid-depth radiocarbon-age difference over the last 20 kyr, Earth Planet. Sc. Lett., 274, 322–326, 2008.

Broecker, W. S., Clark, E., Hajdas, I., and Bonani, G.: Glacial ventilation rates for the deep Pacific Ocean, Paleoceanography, 19, PA2002, doi:10.1029/2003PA000974, 2004a.

Burke, A. and Robinson, L. F.: The Southern Ocean's role in carbon exchange during the last deglaciation, Science 335, 557–561, 2011.

Chang, Y. P., Chen, M. T., Yokoyama, Y., Matsuzaki, H., Thompson, W. G., Kao, S. J., and Kawahata, H.: Monsoon hydrography and productivity changes in the East China Sea during the past 100,000 years: Okinawa Trough evidence (MD012404), Paleoceanography, 24, PA3208, doi:10.1029/2007PA001577, 2009.

Chikamoto, M., Menviel, L., Abe-Ouchi, A., Ohgaito, R., Timmermann, A., Okazaki, Y., Harada, N., Oka, A., and Mouchet, A.: Variability in North Pacific intermediate and deep water ventilation during Heinrich events in two coupled climate models, Deep-Sea Res. Pt. II 61–64, 114–126, 2012.

De Pol-Holz, R., Keigwin, L., Southon, J., Hebbeln, D., and Mohtadi, M.: No signature of abyssal carbon in intermediate waters off Chile during deglaciation, Nat. Geosci., 3, 192–195, 2010.

Elderfield, H., Yu, J., Anand, P., Kiefer, T., and Nyland, B.: Calibrations for benthic foraminiferal Mg/Ca paleothermometry and the carbonate ion hypothesis, Earth Planet. Sc. Lett., 250, 633– 649, 2006.

Feely, R. A., Sabine, C. L., Lee, K., Berelson, W., Kleypas, J., Fabry, V. J., and Millero, F. J.: Impact of anthropogenic CO_2 on the $CaCO_3$ system in the oceans, Science, 305, 362–366, doi:10.1126/science.1097329, 2004.

Galbraith, E. D., Jaccard, S. L., Pedersen, T. F., Sigman, D. M., Haug, G. H., Cook, M., Southon, J. R., and Francois, R.: Carbon dioxide release from the North Pacific abyss during the last deglaciation, Nature, 449, 890–894, 2007.

Graham, D. W., Corliss, B. H., Bender, M. L., and Keigwin, L. D.: Carbon and oxygen isotopic disequilibria of recent deep-sea benthic foraminifera, Mar. Micropaleontol., 6, 483–497, 1981.
Healey, S. L., Thunell, R. C., and Corliss, B. H.: The Mg/Ca–temperature relationship of benthic foraminiferal calcite: new core-top calibrations in the b4 °C temperature range, Earth Planet. Sc. Lett., 272, 523–530, 2008.
Hendy, I. L. and Pedersen, T. F.: Is pore water oxygen content decoupled from productivity on the California Margin? Trace element results from Ocean Drilling Program Hole 1017E, San Lucia slope, California, Paleoceanography, 20, PA4026, doi:10.1029/2004PA001123, 2005.
Horikawa, K., Asahara, Y., Yamamoto, K., and Okazaki, Y.: Intermediate water formation in the Bering Sea during glacial periods: evidence from neodymium isotope ratios, Geology, 38, 435–438, 2010.
Huang, K. F., You, C. F., Chung, C. H., Lin, Y. H., and Liu, Z.: Tracing the Nd isotope evolution of North Pacific intermediate and deep waters through the last deglaciation from South China Sea sediments, J. Asian Earth Sci., 79, 564–573, 2013.
Hut, G.: Consultants Group Meeting on Stable Isotope Reference Samples for Geochemical and Hydrological Investigations Rep. to Dir. Gen., Int. At. Energy Agency, Vienna, 42 pp., 1987.
Itaki, T.: Preliminary report on radiocarbon ages and radiolarian fossils in core GH08-2004 obtained from east off the Okinawa Island, the western Philippine Sea, GSJ Interim report, 51, 171–175, 2010 (in Japanese).
Itaki, T., Katayama, H., Ikehara, K., Suzuki, A., Kaneko, N., Kawamura, N., and Geshi, N.: Bottomo Sediments in east off the Okinawa main island, GSJ Interim report, 46, 47–65, 2009a (in Japanese).
Itaki, T., Katayama, H., Ikehara, K., Suzuki, A., Kawamura, and N., Sato, K.: Oceanographic conditions in east off the Okinawa main island, GSJ Interim report, 46, 66–77, 2009b (in Japanese).
Itaki, T., Katayama, H., Ikehara, K., Suzuki, A., Kaneko, N., Oda, K., and Arai, K.: Bottom sediments in west off the Okinawa main island, GSJ Interim report, 51, 54–68, 2010 (in Japanese).
Itaki, T., Amano, A., Katayama, H., Suzuki, A., Kaneko, Nishida, N., Shimamura, M., Lee, S., and K., and Arai, K.: Bottom sediments in west off the Okinawa main island (around Kume-Zima and Kerama islands), GSJ Interim report, 55, 57–67, 2011a (in Japanese).

CPD
10, 1265–1303, 2014

Variations in intermediate and deep ocean circulation

Y. Kubota et al.

Itaki, T., Amano, A., Katayama, H., and Ikehara, K.: Sediemnt cores in west off the Okinawa main island and their radiocarbon ages, GSJ Interim report, 55, 76–84, 2011b (in Japanese).
Kaneko, I., Takatsuki, Y., and Kamiya, H.: Circulation of intermediate and deep waters in the Philippine Sea, J. Oceanogr., 57, 397–420, 2001.
Keigwin, L. D.: Glacial-age hydrography of the far northwest Pacific, Paleoceanography, 13, 323–339, 1998.
Keigwin, L. D. and Jones, G. A.: Deglacial climate oscillations in the Gulf of California, Paleoceanography, 5, 1009–1023, doi:10.1029/PA005i006p01009, 1990.
Kiefer, T. and Kienast, M.: Patterns of deglacial warming in the Pacific Ocean: a review with emphasis on the time interval of Heinrich event 1: Quaternary Sci. Rev., 24, 1063–1081, doi:10.1016/j.quascirev.2004.02.021, 2005.
Kienast, M., Kienast, S. S., Calvert, S. E., Eglinton, T. I., Mollenhauer, G., Francois, R., and Mix, A. C.: Eastern Pacific cooling and Atlantic overturning circulation during the last deglaciation, Nature, 443, 846–849, 2006.
Kitagawa, H., Fukusawa, H., Nakamura, T., Okamura, M., Takemura, K., Hayashida, A., and Yasuda, Y.: AMS 14C dating of varved sediments from Lake Suigetsu, central Japan and atmospheric ^{14}C change during the late Pleistocene, Radiocarbon, 37, 371–378, 1995.
Komatsu, K., Y. Hiroe, I. Yasuda, K. Kawasaki, T. M. Joyce and F. Bahr: hydrographic structure and transport of intermediate water in the Kuroshio region off the Boso Peninsula, Japan. J. Oceanogr., 60, 487–503, 2004.
Kubota, Y., Kimoto, K., Tada, R., Oda, H., Yokoyama, Y., and Matsuzaki, H.: Variations in East Asian summer monsoon since the last deglaciation based on Mg/Ca and oxygen isotope of planktonic foraminifera in the northern East China Sea, Paleoceanography, 25, PA4205, doi:10.1029/2009PA001891, 2010.
Lea, D. W., Mashiotta, T. A., and Spero, H. J.: Controls on magnesium and strontium uptake in planktonic foraminifera determined by live culturing, Geochim. Cosmochim. Ac., 63, 2369–2379, 1999.
Lear, C. H., Rosenthal, Y., and Slowey, N.: Benthic foraminiferal Mg/Ca paleothermometry: a revised core-top calibration, Geochim. Cosmochim. Ac., 66, 3375–3387, 2002.
Lee, K. E., Lee, H. J., Park, J.-H., Chang, Y.-P., Ikehara, K., Itaki, T., and Kwon, H. K.: Stability of the Kuroshio path with respect to glacial sea level lowering, Geophys. Res. Lett., 40, 1–5, doi:10.1012/grl.50102, 2013.

Lisiecki, L. E.: A simple mixing explanation for late Pleistocene changes in the Pacific-South Atlantic benthic $\delta^{13}C$ gradient, Clim. Past, 6, 305–314, doi:10.5194/cp-6-305-2010, 2010.
Martin, P. A., Lea, D. W., Rosenthal, Y., Shackleton, N. J., Sarnthein, M., and Papenfuss, T.: Quaternary deep sea temperature histories derived from benthic foraminiferal Mg/Ca. Earth Planet. Sc. Lett., 222, 275–283, 2002.
Marchitto, T. M., Lehman, S. J., Ortiz, J. D., Flückiger, J., and van Geen, A.: Marine radiocarbon evidence for the mechanism of deglacial atmospheric CO_2 rise, Science, 316, 1456–1459, 2007a.
Marchitto, T. M., Bryan, S. P., Curry, W. B., and McCorkle, D. C.: Mg/Ca temperature calibration for the benthic foraminifer Cibicidoides pachyderma, Paleoceanography, 22, PA1203, doi:10.1029/2006PA001287, 2007b.
Matsumoto, K., Oba, T., Lynch-Stieglitz, J., and Yamamoto, H.: Interior hydrography and circulation of the glacial Pacific Ocean, Quaternary Sci. Rev., 21, 1693–1704, 2002.
McCorkle, D. C., Keigwin, L. D., Corliss, B. H., and Emerson, S. R.: The influence of microhabitats on the carbon isotopic composition of deep-sea benthic foraminifera, Paleoceanography, 5, 161–185, 1990.
McCorkle, D. C., Corliss, B. H., and Farnham, C. A.: Vertical distributions and stable isotopic compositions of live (stained) benthic foraminifera from the North Carolina and California continental margins, Deep-Sea Res., 44, 983–1024, 1997.
Mekik, F., François, R., and Soon, M.: A novel approach to dissolution correction of Mg/Ca-based paleothermometry in the tropical Pacific, Paleoceanography, 22, PA3217, 2007.
Ohkushi, K., Itaki, T., and Nemoto, N.: Last Glacial–Holocene change in intermediate-water ventilation in the Northwestern Pacific, Quaternary Sci. Rev., 22, 1477–1484, 2003.
Okumura, Y. M., Deser, C., Hu, A., Timmermann, A., and Xie, S.-P.: North Pacific climate response to freshwater forcing in the subarctic North Atlantic: oceanic and atmospheric pathways, J. Climate, 22, 1424–1445, 2009.
Okazaki, Y., Timmermann, A., Menviel, L., Harada, N., Abe-Ouchi, A., Chikamoto, M. O., Mouchet, A., and Asahi, H.: Deepwater formation in the North Pacific during the last glacial termination, Science, 329, 200–204, 2010.
Okazaki, Y., Sagawa, T., Asahi, H., Hoqrikawa, K., and Onodera, J.: Ventilation changes in the western North Pacific since the last glacial period, Clim. Past, 8, 17–24, doi:10.5194/cp-8-17-2012, 2012.

CPD
10, 1265–1303, 2014

Variations in intermediate and deep ocean circulation

Y. Kubota et al.

O'Neil, J. R., Clayton, R. N., and Mayeda, T. K.: Oxygen isotope fractionation in divalent metal carbonates. J. Chem. Phys., 51, 5547–5558, 1969.
Pahnke, K., Goldstein, S. L., Hemming, S. R.: Abrupt changes in Antarctic Intermediate Water circulation over the past 25,000 years. Nat. Geosci., 1, 870–874, doi:10.1038/ngeo360, 2008.
Palmer, M. R. and Pearson, P. N.: A 23,000-year record of surface water pH and pCO$_2$ in the western Equatorial Pacific Ocean, Science, 300, 480–482, 2003.
Pena, L. D., Goldstein, S. L., Hemming, S. R., Jones, K. M., Calvo, E., Pelejero, C., and Cacho, I.: Rapid changes in meridional advection of Southern Ocean intermediate waters to the tropical Pacific during the last 30 kyr, Earth Planet. Sc. Lett., 368, 20–32, 2013.
Qu, T., H. Mitsudera and Yamagata, T.: Intrusion of the North Pacific waters into the South China Sea. J. Geophys. Res., 105, 6415–6424, 2000.
Reid, J. L.: Intermediate waters of the Pacific Ocean, Johns Hopkins Oceanographic Studies, No. 2, 85 pp., 1965.
Reimer, P. J., Baillie, M. G. L., Bard, E., Bayliss, A., Beck, J. W., Blackwell, P. G., Bronk Ramsey, C., Buck, C. E., Burr, G. S., Edwards, R. L., Friedrich, M., Grootes, P. M., Guilderson, T. P., Hajdas, I., Heaton, T. J., Hogg, A. G., Hughen, K. A., Kaiser, K. F., Kromer, B., McCormac, F. G., Manning, S. W., Reimer, R. W., Richards, D. A., Southon, J. R., Talamo, S., Turney, C. S. M., van der Plicht, J., and Weyhenmeyer, C. E.: INTCAL09 and MARINE09 radiocarbon age calibration curves, 0–50,000 years cal BP, Radiocarbon, 51, 1111–1150, 2009.
Rella, S. F., Tada, R., Nagashima, K., Ikehara, M., Itaki, T., Ohkushi, K., Sakamoto, T., Harada, N., and Uchida, M.: Abrupt changes of intermediate water properties on the northeastern slope of the Bering Sea during the last glacial and deglacial period, Paleoceanography, 27, PA3203, doi:10.1029/2011PA002205, 2012.
Roche, D., Paillard, D., Ganopolski, A., and Hoffmann, G.: Oceanic oxygen-18 at the present day and LGM: equilibrium simulations with a coupled climate model of intermediate complexity, Earth Planet. Sc. Lett., 218, 317–330, 2004.
Rosenthal, Y., Boyle, E. A., and Slowey, N.: Temperature control on the incorporation of magnesium, strontium, fluorine, and cadmium into benthic foraminiferal shells from Little Bahamas Bank: prospects for thermocline paleoceanography, Geochim. Cosmochim. Ac., 61, 3633–3643, 1997.

CPD
10, 1265–1303, 2014

Variations in intermediate and deep ocean circulation

Y. Kubota et al.

Sagawa, T. and Ikehara, K.: Intermediate water ventilation change in the subarctic northwest Pacific during the last deglaciation, Geophys. Res. Lett., 35, L24702, doi:10.1029/2008GL035133, 2008.
Sarmiento, J. L., Gruber, N., Brzezinski, M. A., and Dunne, J. P.: High latitude controls of thermocline nutrients and low latitude biological productivity, Nature, 427, 56–60, 2004.
Schlitzer, R.: OceanDataViewSoftware, available at: http://odv.awi.de/, last access: 14 March 2014, 2009.
Schrag, D. P., Adkins, J. F., McIntyre, K., Alexander, J. L., Hodell, D. A., Charles, C. D., and McManus, J. F.: The oxygen isotopic composition of seawater during the Last Glacial Maximum, Quaternary Sci. Rev., 21, 331–342, 2002.
Shackleton, N.: Attainment of isotopic equilibrium between ocean water and the benthonic foraminifera genus Uvigerina: isotopic changes in the ocean during the last glacial, Centre National de la Recherche Scientifique, Coll. Inter, Paris, France, 219, 203–209, 1974.
Skinner, L. C., Fallon, S., Waelbroeck, C., Michel, E., and Barker, S.: Ventilation of the deep Southern Ocean and deglacial CO_2 rise, Science, 328, 1147–1151, 2010.
Spero, H. J. and Lea, D. W.: The cause of carbon isotope minimum events on glacial terminations, Science, 296, 522–525, 2002.
Stommel, H.: Thermohaline convection with two stable regimes of flow, Tellus, 13, 224–230, 1961.
Stott, L., Southon, J., Timmermann, A., and Koutavas, A.: Radiocarbon age anomaly at intermediate water depth in the Pacific Ocean during the last deglaciation, Paleoceanography, 24, PA2223, doi:10.1029/2008PA001690, 2009.
Stuiver, M. and Reimer, P. J.: Extended ^{14}C database and revised CALIB radiocarbon calibration program, Radiocarbon, 35,215–230, 1993.
Sun, Y. B., Oppo, D. W., Xiang, R., Liu, W. G., and Gao, S.: Last deglaciation in the Okinawa Trough: subtropical northwest Pacific link to Northern Hemisphere and tropical climate, Paleoceanography, 20, PA4005, doi:10.1029/2004PA001061, 2005.
Suzuki, A., Ushie, H., Shinmen, K., Amano, A., Kaneko, N., Itaki, T., Katayama, H., Inamura, A., Yasuda, M., Yoshinaga, Y., Murayama, S., and Udami, T.: Geochemical analyses on seawater samples collected during the GH09 cruise in the western off shore of Okinawa Island, GSJ Interim Report, Tsukuba, Japan, 51, 76–85, 2010.
Sverdrup, H., Johnson, M. W., and Fleming, R. H.: The Oceans, Their Physics, Chemistry, and Biology, Prentice-Hall, New York, 1087 pp., 1942.

CPD
10, 1265–1303, 2014

Variations in intermediate and deep ocean circulation

Y. Kubota et al.

Tada, R., Sato, S., Irino, T., Matsui, H., and Kennett, J. P.: Millennialscale compositional variations in late Quaternary sediments at Site 1017, Southern California, Proc. Ocean Drill. Program, Scientific Results, 167, 277–296, doi:10.2973/odp.proc.sr.167.222.2000, 222, 2000.
Talley, L. D.: Distribution and formation of North Pacific intermediate water, J. Phys. Oceanogr., 23, 517–537, 1993.
Talley, L. D.: Antarctic Intermediate Water in the South Atlantic. The South Atlantic: Present and Past Circulation, Springer, Berlin Heidelberg, Germany, 219–238, 1996.
Toggweiler, J. R., Dixon, K., and Broecker, W. S.: The Peru upwelling and the ventilation of the South Pacific thermocline. J. Geophys. Res., 96, 20467–20497, 1991.
Toyofuku, T., Kitazato, H., Kawahata, H., Tsuchiya, M., and Nohara, M.: Evaluation of Mg/Ca thermometry in foraminifera: comparison of experimental results and measurements in nature, Paleoceanography, 15, 456–464, 2000.
Tsuchiya, M. and Talley, L. D.: A Pacific hydrographic section at 881W: water property distribution, J. Geophys. Res., 103, 12899–12918, 1998.
Waelbroeck, C., Labeyrie, L., Michel, E., Duplessy, J. C., McManus, J. F., Lambeck, K., Balbon, E., and Labracherie, M.: Sea level and deep water temperature changes derived from benthic foraminifera isotopic records, Quaternary Sci. Rev., 21, 295–305, doi:10.1016/S0277-3791(01)00101-9, 2002.
Warren, B. A.: Why is no deep water formed in the North Pacific, J. Mar. Res., 41, 327–347, doi:10.1357/002224083788520207,1983.
Wyrtki, K.: The subsurface water masses in the western South Pacific Ocean, Aust. J. Mar. Fresh. Res., 13, 18–47, 1962.
Yasuda, I.: The origin of the North Pacific Intermediate Water, J. Geophys. Res., 102, 893–909. 1997.
Yasuda, I.: North Pacific Intermediate Water: progress in SAGE (Subarctic Gyre Experiment) and related projects, J. Oceanogr., 60, 385–395, 2004.
Yoneda, M., Uno, H., Shibata, Y., Suzuki, R., Kumamoto, Y., Yoshida, K., Sasaki, T., Suzuki, A., and Kawahata, H.: Radiocarbon marine reservoir ages in the western Pacific estimated by pre-bomb molluscan shells, Nucl. Instr. Meth., B, 259, 432–437, 2007.

CPD
10, 1265–1303, 2014

Table 1. The list of the surface K-grab samples and Mg/Ca values of *C. wuellerstorfi* type B. Mg/Ca variability represents a maximum deviation from the mean value of the measurement.

Sampler	Cruise	Sample #	Latitude	Longitude	Description	Water depth (m)	Number of specimen	Bottom water temperature (°C)	Bottom water salinity (°C)	$\delta^{18}O_w$ (‰, VSMOW) (Suzuki et al., 2010)	Average Mg/Ca (mmol mol^{-1})	Mg/Ca Error ± (mmol mol^{-1})
K-grab	GH09	261	26°35.25′ N	127°45.18′ E	grayish olive foraminiferes-bearing mud	336	6	16.31	34.71		3.10	
K-grab	GH09	262	26°37.69′ N	127°41.74′ E	olive yellow mud	346	4	15.89	34.68		2.72	
K-grab	GH09	301	26°45.89′ N	127°51.25′ E	grayshi olive foram-bearing sandy mud	382	9	14.36	34.59		2.73	0.012
Gravity Core	GH10	GH10-2008 Core top	26°47.01′ N	128°49.80′ E	Sandy silt	387	6	13.6	34.45		2.59	
K-grab	GH09	309	26°49.67′ N	127°46.05′ E	olive yellow foram-bearing mud	405	7	13.26	34.53		2.54	0.076
K-grab	GH09	438	26°32.11′ N	127°42.48′ E	olive yellow foraminifers-bearing sandy mud	430	5	13.7	34.55		2.85	0.089
K-grab	GH09	437	26°03.46′ N	127°39.03′ E	olive yellow mud	446	7	13.06	34.5		2.55	0.070
K-grab	GH09	246	26°03.69′ N	127°35.53′ E	olive yellow mud	472	6	12.97	34.52		2.78	
K-grab	GH08	266	26°23.56′ N	128°05.72′ E	grayish olive mud	496	3	11.92	34.4		2.10	0.073
K-grab	GH09	203-2	26°21.98′ N	127°03.17′ E	grayish olive sandy mud	714	7	7.31	34.35		1.69	0.033
K-grab	GH09	454	27°03.54′ N	127°35.56′ E	olive mud	797	7	6	34.39	−0.34	1.33	0.030
K-grab	GH10	424	26°45.02′ N	127°03.65′ E	Dark olive medium sand (0–1.5 cm) and olive gray silt (1.5–2 cm)	959	9	4.7	34.41		1.26	0.028
K-grab	GH08	251	26°14.39′ N	128°11.90′ E	grayish olive foraminifers-bearing mud	968	8	3.74	34.43		1.25	0.010
K-grab	GH09	285	26°52.97′ N	127°02.68′ E	olive mud	1008	7	4.81	34.42	−0.38	1.25	0.051
K-grab	GH10	94	26°24.20′ N	126°52.07′ E	olive silt	1080	4	4.15	34.43		1.16	
K-grab	GH08	214	26°03.01′ N	128°04.27′ E	grayish olive-olive gray foraminifers-bearing mud	1117	9	3.17	34.39		1.05	0.183
K-grab	GH10	185	26°40.36′ N	127°05.21′ E	grayshi olive sandy silt	1294	8	3.93	34.46		1.11	0.027
K-grab	GH08	248	26°24.31′ N	128°26.51′ E	dark olive foraminifers-bearing sandy mud	1369	13	2.58	34.54		1.23	0.045
K-grab	GH08	250	26°12.77′ N	128°16.08′ E	dark grayish yellow foraminifers-bearing mud	1369	10	2.71	34.54		1.08	0.047
K-grab	GH08	207	26°00.08′ N	128°00.62′ E	grayshi olive foraminifers-bearing mud	1455	11, 10[a]	2.51	34.56		1.13	0.22[b]
K-grab	GH08	333	26°27.16′ N	128°33.42′ E	yellowish brown foramnifers-bearing mud	1611	9	2.07	34.51		0.99	0.050
K-grab	GH08	69	25°48.74′ N	127°46.89′ E	grayish yellow foraminifers-bearing sandy mud	1774	6	2.17	34.58		1.05	
K-grab	GH08	332	26°22.00′ N	128°03.25′ E	yellowish brown foraminifers-bearing sandy mud	1952	11	2.09	34.56		0.85	0.009
K-grab	GH08	331	26°22.34′ N	128°40.41′ E	yellowish brown foraminifers-bearing mud	2195	4, 2[a]	1.83	34.59		0.88	0.048[b]
K-grab	GH08	198	25°54.37′ N	128°11.89′ E	grayish olive foraminifers-bearing sandy mud	2201	2	1.84	34.64		0.83	0.058
K-grab	GH08	50	25°39.81′ N	127°45.49′ E	grayish yellow foraminifers-bearing mud	2281	3	1.88	34.63		0.91	
K-grab	GH08	197	26°05.01′ N	128°36.02′ E	grayish olive foraminifers-bearing mud	2679	6	1.65	34.66		1.13	0.176

[a] = the foraminiferal tests were repicked and rerun for duplication test of Mg/Ca.
[b] = maximum deviation from the average of the duplicated analysis.

Table 2. Radiocarbon ages of planktic foraminifers and an age of the tephra from core GH08-2004.

	Depth [cm]	Species	Conventional ^{14}C age [yr]	error ±	Calendar age [yr BP]	error ± (1σ)	error ± (2σ)	Lab code
Planktic foraminifers	19.3–21.4	*G. menardii*	3530	40	3382.5	45.5	117.5	Beta-260492[a]
	23.6–25.7	*G. sacculifer*	4540	170	4725.5	286.5	477.5	MTC-13738
	40.5–42.7	*G. sacculifer and G. ruber*	6450	40	6902.5	62.5	134.5	Beta-293085[b]
	67.3–69.5	*G. sacculifer*	8265	100	8753	127	269	MTC-13739
	80.7–82.9	*G. ruber*	9320	40	10 077.5	2.5	134.5	Beta-344154[a]
	127.6–129.8	*G. ruber*	11 660	50	13 091.5	21.5	176.5	Beta-344155
	134.3–136.0	*G. sacculifer*	12 265	110	13 661.5	154.5	248.5	MCT-13741
	142.9–145.2	*G. truncatulinoides*	12 940	70	14 635.5	382.5	445.5	Beta-260494[a]
	172.8–175.1	*G. sacculifer*	14 955	115	17 599	93	390	MCT-13742
	225.6–227.9	*G. truncatulinoides*	18 780	100	21 884	226	371	Beta-260495
Ash layer[c]	43	K-Ah			7300			

[a] = ^{14}C data from Itaki (2010).
[b] = ^{14}C data from Itaki et al. (2011b).
[c] = the age of K-Ah from Kitagawa et al. (1995).

CPD
10, 1265–1303, 2014

Variations in intermediate and deep ocean circulation

Y. Kubota et al.

Title Page
Abstract Introduction
Conclusions References
Tables Figures
◀| |▶
◀ ▶
Back Close
Full Screen / Esc
Printer-friendly Version
Interactive Discussion

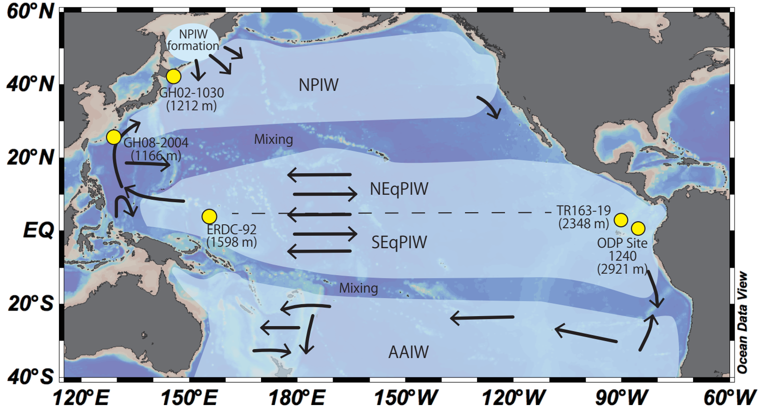

Fig. 1. Map of formation regions of North Pacific Intermediate Water (NPIW) and distribution of the intermediate waters in the Pacific (modified from Bostock et al., 2010). The intermediate waters are Antarctic Intermediate Water (AAIW), North Equatorial Pacific Intermediate Water (NEqPIW), South Equatorial Pacific Intermediate Water (SEqPIW), and NPIW. Arrows show the possible flow of intermediate depth waters (Bostock et al., 2010). The location of the sediment cores discussed in the text is also shown.

CPD
10, 1265–1303, 2014

Variations in intermediate and deep ocean circulation

Y. Kubota et al.

Title Page
Abstract Introduction
Conclusions References
Tables Figures
◂◂ ▸▸
◂ ▸
Back Close
Full Screen / Esc
Printer-friendly Version
Interactive Discussion

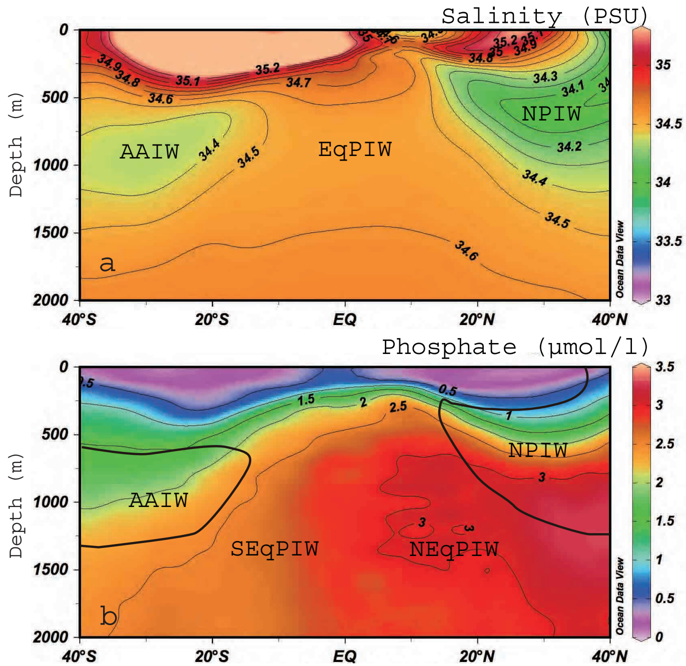

Fig. 2. Transects along 170° W: **(a)** salinity vs. depth (0–2000 m), indicating the North Pacific Intermediate Water (NPIW), Antarctic Intermediate Water (AAIW), North Equatorial Pacific Intermediate Water (NEqPIW), and South Equatorial Pacific Intermediate Water (SEqPIW). **(b)** Phosphate concentration vs. depth. Figures are made with Ocean Data View (Schlitzer, 2009).

CPD
10, 1265–1303, 2014

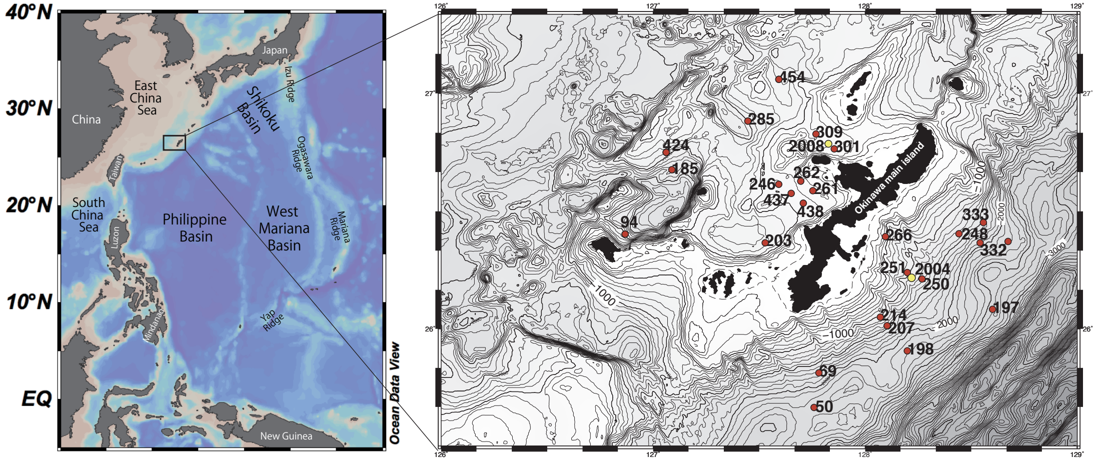

Fig. 3. Map showing the locations of surface sediment samples and core GH10-2008 used for Mg/Ca calibration and core GH08-2004.

CPD
10, 1265–1303, 2014

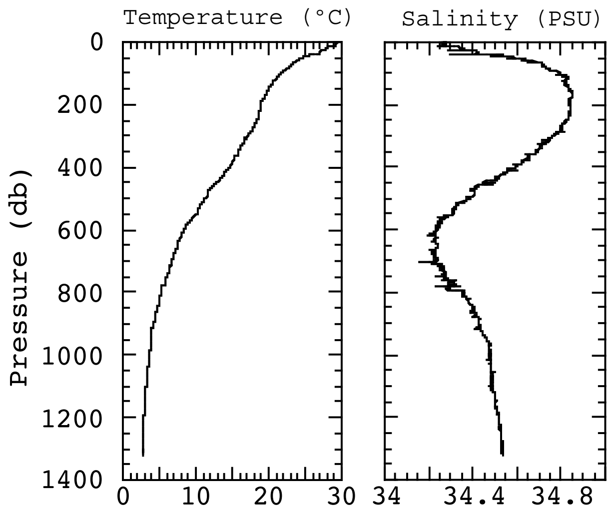

Fig. 4. Temperature and salinity profile vs. depth at site 250 (26°12.77′ N, 128°16.08′ E) measured by CTD during GH08 cruise (Itaki et al., 2009).

CPD
10, 1265–1303, 2014

Variations in intermediate and deep ocean circulation

Y. Kubota et al.

Title Page
Abstract Introduction
Conclusions References
Tables Figures
◀◀ ▶▶
◀ ▶
Back Close
Full Screen / Esc
Printer-friendly Version
Interactive Discussion

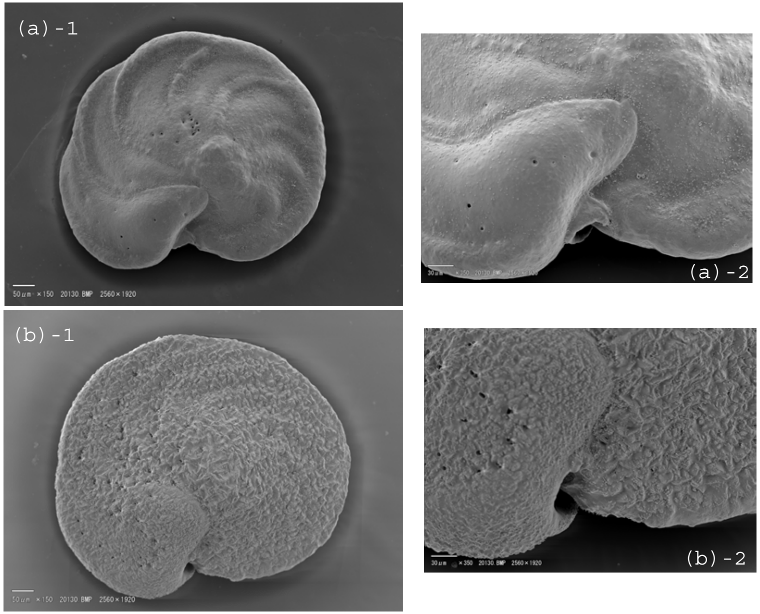

Fig. 5. SEM images of *C. wuellerstorfi* type A, sensu stricto **(a)**-1 and **(a)**-2, and *C. wuellerstorfi* type B **(b)**-1 and **(b)**-2.

CPD
10, 1265–1303, 2014

Variations in intermediate and deep ocean circulation

Y. Kubota et al.

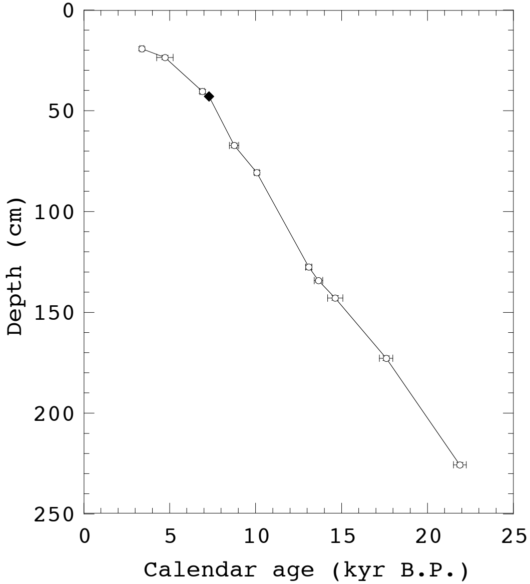

Fig. 6. Age model of GH08-2004. Open symbols represent the ^{14}C data and 2σ errors. The filled symbol represents the K–Ah tephra.

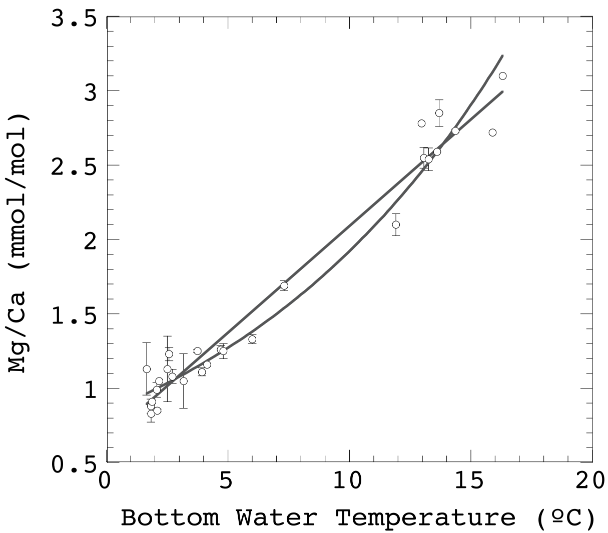

Fig. 7. Bottom water temperatures (BWT) vs. Mg/Ca values of surface sediment samples (K-grab) and a core top sample.

CPD
10, 1265–1303, 2014

Title Page
Abstract
Introduction
Conclusions
References
Tables
Figures
Back
Close
Full Screen / Esc
Printer-friendly Version
Interactive Discussion

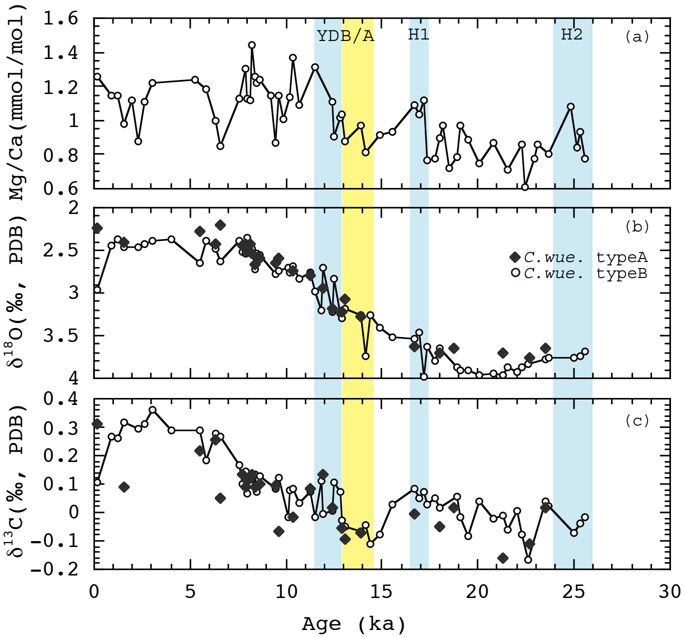

Fig. 8. (a) Mg/Ca, **(b)** $\delta^{18}O_c$ and **(c)** $\delta^{13}C_c$ vs. calendar age for GH08-2004. **(b)** and **(c)** Filled diamonds represent benthic $\delta^{18}O_c$ and $\delta^{13}C_c$ data from *C. wuellerstorfi* type A, and open circles represent *C. wuellerstorfi* type B. H1, B/A, and YD represent Heinrich 1, Bølling/Allerød, and Younger Dryas intervals defined by Wang et al. (2006) and Stanford et al. (2006).

CPD

10, 1265–1303, 2014

Variations in intermediate and deep ocean circulation

Y. Kubota et al.

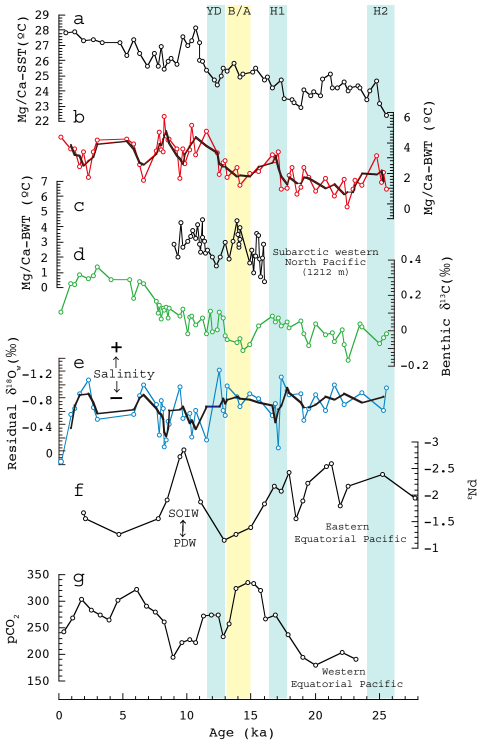

Fig. 9. **(a)** Sea surface temperature (SST) derived from Mg/Ca of the planktic foraminifera *G. ruber* of core GH08-2004 (Lee et al., 2004), **(b)** bottom water temperature (BWT) derived from Mg/Ca of the benthic foraminifera *C. wuellerstorfi* of core GH08-2004 (this study), **(c)** Mg/Ca-derived BWT of *U. akitaensis* of core GH02-1030, 1212 m water depth in the subarctic western North Pacific (Sagawa and Ikehara, 2008), **(d)** benthic $\delta^{13}C$ of GH08-2004 (this study), **(e)** residual $\delta^{18}O_w$($\Delta\delta^{18}O_w$) of GH08-2004 (this study), **(f)** Nd isotope ratio (ε_{Nd}) of ODP site 1240 which reflects the contribution of the Pacific Deep Water (PDW) and Southern Ocean Intermediate Water (SOIW) such as AAIW and Subantarctic Mode Water (Pena et al., 2013), and **(f)** pCO_2 reconstruction based on Boron isotope ($\delta^{11}B$) of core ERDC-92 from the western equatorial Pacific (Palmer and Pearson, 2003). H2, H1, B/A, and YD represent Heinrich 2, Heinrich 1, Bølling/Allerød, and Younger Dryas intervals defined by Wang et al. (2006) and Stanford et al. (2006).

CPD
10, 1265–1303, 2014

Variations in intermediate and deep ocean circulation

Y. Kubota et al.